Turning copper metal into a Weyl semimetal

Yongping Du and Er-jun Kan
Department of Applied Physics and Institution of Energy and Microstructure Nanjing University of Science and Technology, Nanjing, Jiangsu 210094, People's Republic of China

Hu Xu
Department of Physics, South University of Science and Technology of China, Shenzhen 518055, China

Sergey Y. Savrasov*
Department of Physics, University of California, Davis, California 95616, USA

Xiangang Wan†
National Laboratory of Solid State Microstructures and Department of Physics, Nanjing University, Nanjing 210093, China and Collaborative Innovation Center of Advanced Microstructures, Nanjing University, Nanjing 210093, China

(Received 30 January 2018; published 5 June 2018)

A search for new topological quantum systems is challenging due to the requirement of nontrivial band connectivity that leads to protected surface states of electrons. Progress in this field was primarily due to a realization of a band inversion mechanism between even and odd parity states that was proven to be very useful in both predicting many such systems and our understanding of their topological properties. Despite many proposed materials that assume the band inversion between s and p (or p/d, d/f) electrons, here, we explore a different mechanism where the occupied d states subjected to a tetrahedral crystal field produce an active t_{2g} manifold behaving as a state with an effective orbital momentum equal to -1, and pushing $j_{\text{eff}} = 1/2$ doublet at a higher energy. Via hybridization with nearest-neighbor orbitals realizable, e.g., in a zinc-blende structural environment, this allows a formation of odd parity state whose subsequent band inversion with an unoccupied s band becomes possible, prompting us to look for the compounds with Cu^{+1} ionic state. Chemical valence arguments coupled to a search in the materials database of zinc-blende-like lattice space groups T_d^2 ($F\bar{4}3m$) lead us to systematically investigate electronic structures and topological properties of CuY (Y = F, Cl, Br, I) and CuXO (X = Li, Na, K, Rb) families of compounds. Our theoretical results show that CuF displays a behavior characteristic of an ideal Weyl semimetal with 24 Weyl nodes at the bulk Brillouin zone. We also find that other compounds, CuNaO and CuLiO, are the s-d inversion-type topological insulators. Results for their electronic structures and corresponding surfaces states are presented and discussed in the context of their topological properties.

DOI: 10.1103/PhysRevB.97.245104

I. INTRODUCTION

Topological quantum solids are a new class of systems that behave as an insulator or semimetal in the bulk but whose surface contains conducting states meaning that the electrons can primarily move along the surface of the material. Starting from the original proposal on the principal existence of such state of matter in the case of two dimensions called a quantum spin Hall insulator [1,2] and its subsequent extension to its three-dimensional (3D) analog called a topological insulator (TI) [3], the field has been recently enriched by the discoveries of new topological phases of matter such as topological crystalline insulators [4], Weyl semimetals (WSMs) [5], Dirac semimetals (DSMs) [6–8], and nodal line semimetals (NLSs) [9]. Their unusual properties such as robust surface currents insensitive to the disorder or various forms of quantum Hall effects have led to a plethora of proposals for the use of topological materials in fundamental research spanning from magnetic monopoles to Majorana fermions, and in applications such as fault-tolerant quantum computations [10,11].

How do we identify new topological materials in the infinite world of chemically allowed compounds? Although group-theoretical arguments have been recently shown to be very helpful in our understanding of band connectivity and their resulting topological behavior [12,13], the remarkable progress in this field has been primarily driven by a realization of the so-called band inversion mechanism [2] where the s level at the conduction-band edge and the p level at the valence-band edge interchange at a certain portion of the Brillouin zone (BZ) and open a hybridization gap. Since s and p are even or odd parity states, this may result in a nonzero Z_2 topological invariant according to the Fu-Kane criterion of the 3D TIs [14]. Much celebrated discoveries of such topological systems as HgTe quantum wells [2], Bi_2Se_3 and related compounds [15,16], proposals for half-Heusler ternary compounds [17–19], $BaBiO_3$ [20], etc., have been all based on this band

*savrasov@physics.ucdavis.edu
†xgwan@nju.edu.cn

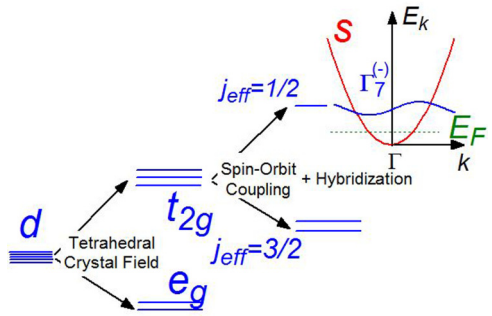

FIG. 1. Illustration of how the atomic d level subjected to a tetrahedral crystal-field spin-orbit coupling and hybridization with nearest neighbors produces odd parity $\Gamma_7^{(-)}$ doublet that can hybridize with a predominantly empty s band of a material.

inversion mechanism. Very interesting extensions of these ideas for the inversion between d and f levels have led to the proposals of some americium and plutonium compounds [21] showing nontrivial topological properties as well as to the discovery of a topological Kondo insulator SmB_6 [22]. Another example is the most recent proposal of nodal line materials that have the p-d inversion of levels [23–26].

Will systems with hybridized s and d electrons qualify to show topologically protected states? Despite that the corresponding spherical harmonics are both of even parity, it is well known that the d states subjected to the cubic crystal field produce a t_{2g} triplet that behaves in many cases as a state with effective orbital momentum equal to -1 [27]. Most notable examples here are the Mott insulating behavior in Sr_2IrO_4 [28] and predicted noncollinear magnetism in pyrochlore iridates [5] where the spin-orbit splitting of the t_{2g} manifold leads to an active $j_{\rm eff} = 1/2$ doublet state. One can subsequently explore a different class of materials where active s and d electrons realize interesting topologically nontrivial systems. This is schematically illustrated in Fig. 1 where the atomic d level is subjected to a tetrahedral crystal field realizable, e.g., in a zinc-blende structural environment, and spin-orbit coupling can form an odd parity $\Gamma_7^{(-)}$ state via hybridization with nearest-neighbor orbitals. A subsequent band inversion with an unoccupied s band becomes possible in compounds containing ionic configurations $d^{10}s^0$, such as Cu^{+1}.

Here we report on a theoretical study of how such a s-d inversion mechanism is capable to produce topologically nontrivial electronic phases and lead to different realizations of Weyl semimetals and topological insulators. First, we use a low-energy kp model to illustrate the parameter space responsible for the appearance of various topological phases. Second, using a valence argument, we establish a chemical space of relevant compounds, and by coupling first-principles band-structure calculations with a search in the materials database, we successfully predict that CuF is a Weyl semimetal with 24 Weyl points in the bulk Brillouin zone. Remarkably, this material does not show any other trivial states crossing the Fermi level contrary to recently discovered TaAs [29,30] and other WSMs [11]. Furthermore, we also predict that CuNaO and CuLiO are the s-d inversion-type topological insulators.

II. RESULTS AND DISCUSSION

Effective model. The d orbital subjected to a crystal field of cubic lattices is split onto t_{2g} and e_g orbital states, where, if the local symmetry is octahedral, the energy of e_g state comes higher than the one of t_{2g} state, while if the local symmetry is tetrahedral, the energy of the t_{2g} is higher than the one of the e_g. Within the t_{2g} manifold, the effective orbital angular momentum is one with an additional minus sign [27]. That means that when the spin-orbit coupling (SOC) of the strength λ is taken into account, the t_{2g} state is split into an effective $j_{\rm eff} = 1/2$ doublet state with energy λ and a $j_{\rm eff} = 3/2$ quadruplet state with energy $-\lambda/2$. Note that the $j_{\rm eff} = 1/2$ state is energetically higher than the $j_{\rm eff} = 3/2$. Allowing hybridization with nearest-neighbor orbitals the $j_{\rm eff} = 1/2$ doublet can form an antibonding state of odd parity, $|\Gamma_7^{(-)}\rangle$. Thus, as we illustrate in Fig. 1, if a predominantly empty band of the even parity (s) character resides above the occupied d level, its bottom around the Γ point and odd parity $\Gamma_7^{(-)}$ state can interchange and open a hybridization gap. This scenario may produce a nonzero Z_2 topological invariant because according to the Fu and Kane criterion [14], the product of occupied states parities at all time-reversal invariant momenta becomes equal to -1 due to the occurrence of the band inversion around the Γ point.

Although many lattice space groups would qualify for exploring this idea, the ones without inversion symmetry are particularly interesting since they are capable of realizing Weyl semimetals. These materials were recently proposed to have topological surface states in a form of Fermi arcs [5] as well as a great number of other exotic phenomena such as a highly anisotropic negative magnetoresistance related to chiral anomaly effect [31,32], a topological response [33], unusual nonlocal transport properties [34], interesting quantum oscillations from the Fermi arcs [35], etc. [11].

One of the simplest structures that would fit the requirement of the absent inversion center is the zinc-blende structure with the space group T_d^2 ($F\bar{4}3m$). Let us use a kp method and construct a low-energy effective model around the Γ point in the symmetry of the zinc-blende structure by considering only a minimal basis set of four orbitals: $|s, j_z = 1/2\rangle$, $|s, j_z = -1/2\rangle$, $|\Gamma_7^{(-)}, j_z = 1/2\rangle$, $|\Gamma_7^{(-)}, j_z = -1/2\rangle$.

The Hamiltonian reads

$$H_{\rm eff} = \epsilon_0(\mathbf{k}) + \begin{pmatrix} M(\mathbf{k}) & 0 & Pk_z + iVk_xk_y & Pk_- + Vk_zk_+ \\ 0 & M(\mathbf{k}) & Pk_+ - Vk_zk_- & -Pk_z - iVk_xk_y \\ Pk_z - iVk_xk_y & Pk_- - Vk_zk_+ & -M(\mathbf{k}) & 0 \\ Pk_+ + Vk_zk_- & -Pk_z + iVk_xk_y & 0 & -M(\mathbf{k}) \end{pmatrix},$$

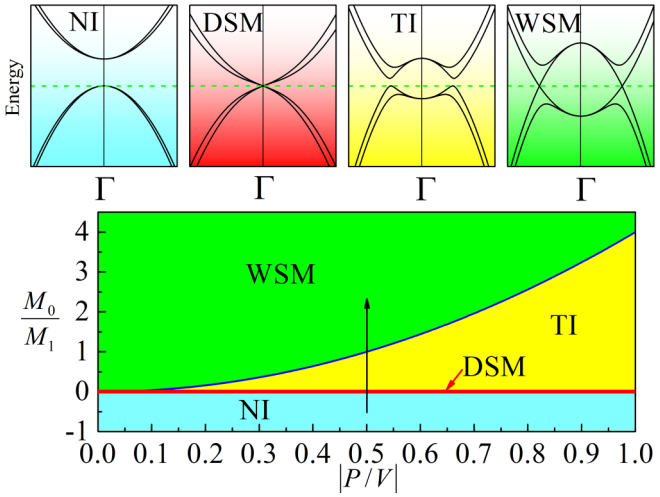

FIG. 2. Phase diagram of the minimal $(4 \times 4)\,kp$ model involving two s orbitals and two $\Gamma_7^{(-)}$ orbitals in the symmetry T_d^2 ($F\bar{4}3m$) of the zinc-blende structure which illustrates realization of various topological phases in the parameter space of the model: normal insulator (NI) (cyan), Dirac semimetal (DSM) (red), topological insulator (TI) (yellow), Weyl semimetal (WSM) (green).

where $k_\pm = k_x \pm ik_y$ and $M(\mathbf{k}) = M_0 - M_1\mathbf{k}^2$ with parameters M_0, M_1 chosen to be less than zero in order to reproduce the band inversion. In such a case, the energy dispersion is $E(\mathbf{k}) = \epsilon_0(\mathbf{k}) \pm \sqrt{A(\mathbf{k})^2 + B_\pm(\mathbf{k})^2}$, where $A(\mathbf{k})^2 = M(\mathbf{k})^2$, $B_\pm(\mathbf{k})^2 = P^2\mathbf{k}^2 + V^2(k_x^2k_y^2 + k_x^2k_z^2 + k_y^2k_z^2) \pm 2\sqrt{P^2V^2[k_y^2(k_x^2 - k_z^2)^2 + k_x^2(k_y^2 - k_z^2)^2 + k_z^2(k_x^2 - k_y^2)^2]}$. The band crossing points are given by the following conditions: $A(\mathbf{k})^2 + B_-(\mathbf{k})^2 = 0$.

According to the conditions of the band inversion and the band crossings, we can obtain the phase diagram with a variety of topological phases such as DSM, WSM, and TI, depending on the parameters of the model. This is illustrated in Fig. 2. For example, let us fix the parameter $|\frac{P}{V}| = 0.5$ and alter $\frac{M_0}{M_1}$, as shown by a vertical arrow in Fig. 2. For any $\frac{M_0}{M_1} < 0$, there is no band inversion, and the system is a normal insulator (NI), because the s band is higher than the $\Gamma_7^{(-)}$ band everywhere in k space. When $\frac{M_0}{M_1}$ approaches zero, the s band lowers down, and when $\frac{M_0}{M_1} = 0$, the s band exactly touches the $\Gamma_7^{(-)}$ band at the Γ point. The system becomes a Dirac semimetal with fourfold degenerate Dirac point exactly at $\mathbf{k} = 0$. The DSM plays the role of a phase boundary between topologically trivial and nontrivial phases. It is indeed a line in the phase diagram (red) for any value of $|\frac{P}{V}|$. If we further lower the s band by increasing $\frac{M_0}{M_1}$ (both M_0, $M_1 < 0$), the band inversion occurs. First, we obtain the TI phase, and, second, the ideal WSM emerges. The Weyl points are confined within $k_x = 0$, $k_y = 0$, or $k_z = 0$ planes by a special symmetry $C_{2T} = C_2T$ where C_2 denotes twofold rotation C_{2x}, C_{2y}, and C_{2z} and T denote the time-reversal symmetry [36].

To illustrate the transition between the TI and the WSM phases, let us set $k_z = 0$. Then the condition for bands crossing, $A(\mathbf{k})^2 + B_-(\mathbf{k})^2 = 0$, requires both $A(\mathbf{k}) = 0$ and $B_-(\mathbf{k}) = 0$, where $A(\mathbf{k}) = M_0 - M_1(k_x^2 + k_y^2)$ and $B_-(\mathbf{k}) = |P||\sqrt{k_x^2 + k_y^2}| - |V||k_xk_y|$. $A(\mathbf{k}) = 0$ is the equation for a circle and $B_-(\mathbf{k}) = 0$ is a hyperbolic equation. When $M_0 = 0$, the circle becomes a point and the band crossing occurs at $\mathbf{k} = 0$ giving rise to the DSM phase. When $M_0 < 0$, the band crossing is determined by the crossing between the circle and the hyperbola. Touching between the two occurs at $\frac{M_0}{M_1} = 4|\frac{P}{V}|^2$, which is the boundary between the TI and the WSM phases.

Material realization. A realization of such a model dictates the search of a material with a fully occupied narrow d band and an empty wide s band, so that, in principle, any ionic compound with Cu^{+1} valence state subjected to the discussed symmetry constraints qualifies. We therefore utilize a first-principles electronic structure method (for details, see the Appendix) and systematically investigate energy bands and topological properties of the following two families of compounds: CuX (X = F, Cl, Br, I) and CuYO (Y = Li, Na, K, Rb). Our results indicate that the compound CuF is an ideal Weyl semimetal while CuNaO and CuLiO are both topological insulators of the discussed s-d-type band inversion.

We first discuss electronic structures of CuX (X = F, Cl, Br, I) family [37]. Experimentally, it was reported in 1933 that CuF crystallizes in a zinc-blende structure [37], illustrated in Fig. 3(a), although its existence under ambient conditions was questioned later on [37–41]. As there are no free internal coordinates in this type of structure, the only parameters to optimize are the lattice constants. Our numerical results are in good agreement with the original experimental work [37] and small discrepancies have a negligible effect on the electronic structures.

Our theoretical analysis shows that the compounds CuCl, CuBr, CuI are all topologically trivial band insulators. The band structure of CuF along two high-symmetry lines of the first BZ [for notations, see Fig. 3(b)] is shown in Fig. 3(c). The spin-orbit coupling is included in the calculation. Our orbital-character analysis confirms that the states near the Fermi level are mainly formed by Cu-3d states (denoted by blue color) and Cu-4s states (denoted by red color) as shown in Fig. 3(c). F-2p states are located between -8.5 and -7.5 eV indicating that they are far away from the Fermi level. However, they hybridize strongly with nearest-neighbor Cu $j_{eff} = 1/2$ states and produce an antibonding odd-parity doublet $\Gamma_7^{(-)}$. To illustrate this, in the inset of Fig. 3(c), we plot the calculated wave function $|\Gamma_7^{(-)}\rangle$ along the line connecting Cu and F atoms. One can clearly see that, at the Cu site, the wave function is even but in the middle of the Cu-F bond, it becomes odd via the formation of the antibonding combination between Cu $j_{eff} = 1/2$ and F $2p$. We find that apart from the linearly dispersing Weyl states there are no other bands crossing the Fermi level. We also find that the $\Gamma_7^{(-)}$ state located at 0.04 eV above the Fermi energy and the Cu-4s state located at -0.47 eV form an inverted band structure around the Γ point.

Our further calculation reveals that CuF is an ideal Weyl semimetal without any additional Fermi pockets. The Weyl points are searched for by scanning the whole BZ. To check their locations, the Chern number associated with each Weyl point is calculated by integrating the Berry curvature based on a computational scheme proposed by Fukui *et al.* [42]. We find that the locations of the Weyl nodes with chirality $C = +1$ are

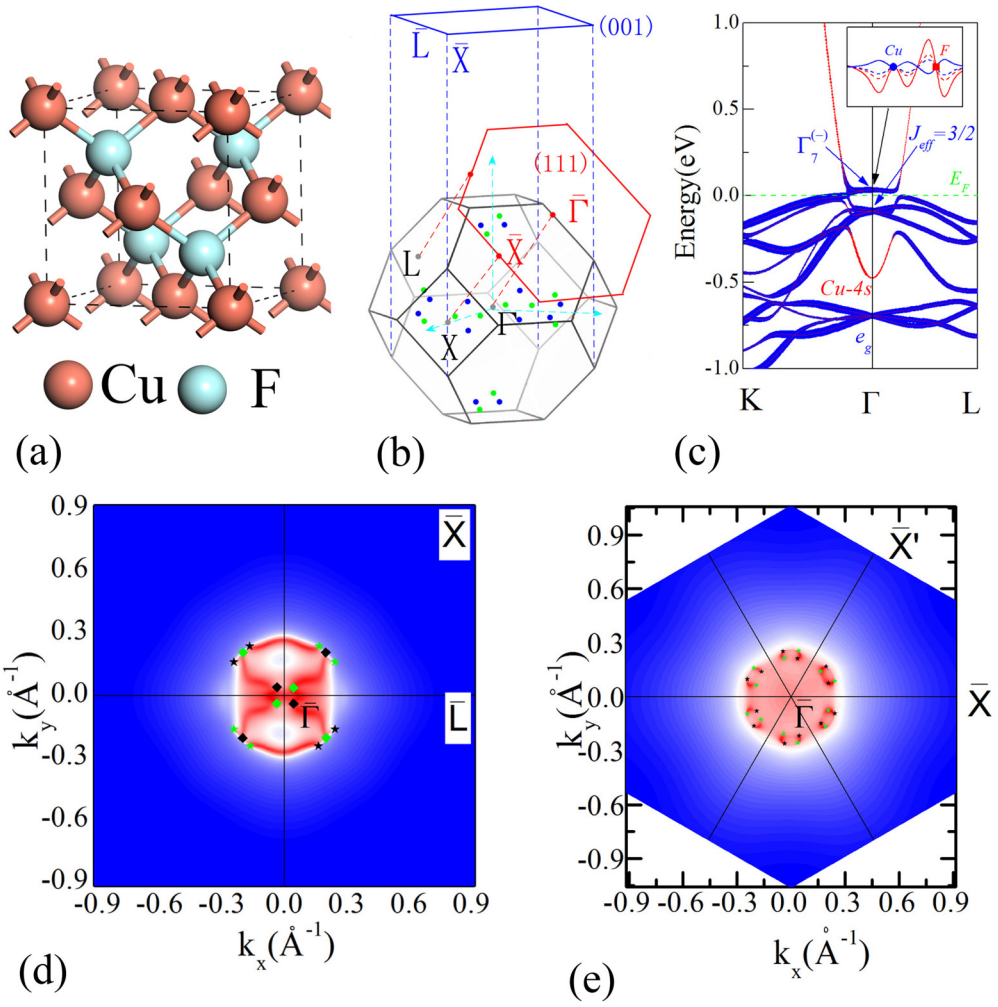

FIG. 3. Results for CuF: (a) Crystal structure with Cu atoms (red) and F atoms (cyan). (b) Brillouin zone and the projected (001) (blue) and (111) (red) surfaces. Green (with Chern number $+1$) and blue (with Chern number -1) dots show schematic positions of the Weyl nodes. (c) Band structure in the vicinity of the Fermi level where $\Gamma_7^{(-)}$ states (blue) and s states (red) form band inversion. The inset shows a wave function $|\Gamma_7^{(-)}\rangle$ along the Cu-F line, behaving as an odd parity state with respect to the point approximately midway between Cu and F. Solid/dashed lines show real (red) and imaginary (blue) parts of two components of $\Gamma_7^{(-)}$, respectively. (d) The Fermi arc surface states for the (001) surface. (e) Fermi arc surface states for (111) surface. Here the green (black) diamonds are the projections of two Weyl points with monopole charges $+2$ (-2), while the green (black) stars are the projections of the single Weyl point with monopole charges $+1$ (-1).

$(\pm k_1, \pm k_2, 0), (0, \pm k_1, \pm k_2), (\pm k_2, 0, \pm k_1)$, and those with chirality $C = -1$ are $(\pm k_1, 0, \pm k_2), (\pm k_2, \pm k_1, 0), (0, \pm k_2, \pm k_1)$, where $k_1 = 0.205\,11$ Å^{-1} and $k_2 = 0.051\,14$ Å^{-1}. There are a total of 24 Weyl nodes related by C_3 rotational symmetry along the [111] direction and C_2 rotational symmetry in the first BZ, as shown schematically in Fig. 3(b). They are confined within $k_x = 0$, $k_y = 0$, and $k_z = 0$ planes by the coexistence of time-reversal symmetry and the twofold rotations, i.e., C_{2T} [36].

The existence of novel Fermi arc surface states is a remarkable feature of Weyl semimetals. In an ideal case, such as the one we find for CuF, a well separated set of Weyl nodes only exists at the Fermi level, and leads to long Fermi arcs. To illustrate this, we calculate surface states of CuF by using the Green-function method based on the tightbinding Hamiltonian obtained from maximally localized Wannier functions (MLWFs) fit to the first-principles calculation [43]. The Fermi arc surface states for the (001) and (111) surfaces are shown in Figs. 3(d) and 3(e), respectively.

In particular, for the (001) surface, the arcs are found to be long and should be easily detectable experimentally. In Fig. 3(d), there are two touching points along $\bar{\Gamma}$-$\bar{X}$ which originate from the two Weyl points, with monopole charges $+2$ (green diamonds) and -2 (black diamonds). Therefore, one can clearly see two surface states coming out from these Weyl points. Along $\bar{\Gamma}$-$\bar{L}$, there are no projected Weyl points, but there exists a surface state crossing the Fermi level which indicates a Fermi arc crossing $\bar{\Gamma}$-$\bar{L}$. The green (black) diamonds here represent the projection of two Weyl points with monopole charges $+2$ (-2), while the green (black) stars represent the single Weyl point projection with monopole charge $+1$ (-1).

The compounds CuYO (Y = Li, Na, K, Rb) have first been reported to exist in a tetragonal structure with space group $I4/mmm$ [44]. However, a recent theoretical work also showed that under high hydrostatic pressure CuYO (Y = Li, Na, K, Rb) can undergo a structural phase transition to a zinc-blende structure [45] which is at the center of interest in our work.

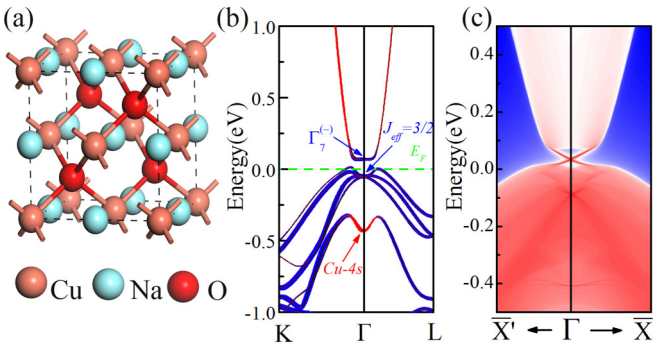

FIG. 4. Results for CuNaO: (a) Crystal structure where light red spheres denote Cu atoms, dark red spheres denote O atoms, and the cyan spheres denote Na atoms. (b) Band structure in the vicinity of the Fermi level where Cu $j_{\text{eff}}^{\text{ant}} = 1/2$ states (blue) and Cu 4s states (red) form band inversion. (c) Dirac cone surface states for the (111) surface.

Our electronic structure calculations are performed with lattice parameters consistent with the previous theoretical studies [45,46]. Our numerical results show that CuLiO and CuNaO are both topological insulators while CuKO and CuRbO are normal insulators.

Let us take CuNaO as an example showing unique features of the s-d inversion mechanism. Its crystal structure is illustrated in Fig. 4(a). The electronic structure with SOC included is shown in Fig. 4(b). The active states around the Fermi level are the Cu-3d states (blue) and Cu-4s states (red). From the details at the Γ point, the $\Gamma_7^{(-)}$ states are located at $+0.07$ eV while the 4s states are at -0.43 eV. This illustrates the band inversion mechanism. Our calculation of Z_2 topological invariant verifies that this system is a TI. The corresponding band-structure calculation for the (111) surface is shown in Fig. 4(c) where a linearly dispersing Dirac cone is resolved within a small bulk energy gap.

III. CONCLUSION

In conclusion, we have explored the band inversion mechanism between spin-orbit coupled t_{2g} states and a wide s band for a zinc-blende-type structure. We found that a few ionic compounds with Cu^{+1} valence state exhibit nontrivial topological properties: CuLiO and CuNaO are the topological insulators while CuF is a Weyl semimetal. Remarkably, apart from the Weyl nodes, there are no other Fermi surface states in this compound which makes it appealing for further experimental studies of such effects as a large negative magnetoresistance. Being a definite signature of the chiral anomaly in the quantum limit, it has been observed in known Weyl semimetals [47], but it is not clear how to separate contributions from the Weyl points and regular Fermi pockets.

Our theoretical work demonstrates how the ideas of band inversion coupled to chemical valence considerations can guide the search of new topological quantum systems in the infinite database of materials. Although the tight-binding method employed in our work to detect Fermi arc surface states does not take into account surface relaxation effects, it shows the existence of long arcs in CuF. We have recently shown [48], that long and straight Fermi arcs are generally capable of supporting nearly dissipationless surface currents, therefore it could be interesting to explore if nanowires based on CuF are realizable in practice.

ACKNOWLEDGMENTS

The work was supported by National Key R&D Program of China (Grants No. 2017YFA0303203 and No. 2018YFA0305700), the National Natural Science Foundation of China (Grants No. 11525417, No. 51572085, No. 51721001, and No. 11790311), National Key Project for Basic Research of China (Grant No. 2014CB921104), the Priority Academic Program Development of Jiangsu Higher Education Institutions. Y.P.D. was supported by the Natural Science Foundation of Jiangsu Province (Grant No. BK20170821), and the Special Foundation for Theoretical Physics Research Program of China (Grant No. 11747165). S.Y.S. was supported by NSF DMR (Grant No. 1411336).

APPENDIX: COMPUTATIONAL DETAILS

We perform first-principles calculations based on the full potential linearized augmented plane wave (FP-LAPW) method as implemented in WIEN2K package [49]. To obtain accurate band inversion strength and band order, the modified Becke-Johnson exchange potential together with local-density approximation for the correlation potential (MBJLDA) has been used [50]. The plane-wave cutoff parameter $R_{MT}K_{\max}$ is set to be 7. The spin-orbit coupling is treated using the second-order variational procedure. To check the existence of the Weyl nodes, a dense k mesh with $24 \times 24 \times 24$ divisions of reciprocal-lattice translations has been employed. To study the surface states, we use the Green's-function method based on a tight-binding Hamiltonian using the maximally localized Wannier functions (MLWFs), which are projected from the Bloch states derived from first-principles calculations [43].

[1] C. L. Kane and E. J. Mele, Quantum Spin Hall Effect in Graphene, Phys. Rev. Lett. **95**, 226801 (2005).
[2] B. A. Bernevig, T. L. Hughes, and S.-C. Zhang, Quantum spin Hall effect and topological phase transition in HgTe quantum wells, Science **314**, 1757 (2006).
[3] C. L. Kane and E. J. Mele, Z_2 Topological Order and the Quantum Spin Hall Effect, Phys. Rev. Lett. **95**, 146802 (2005).
[4] L. Fu, Topological Crystalline Insulators, Phys. Rev. Lett. **106**, 106802 (2011).
[5] X. Wan, A. M. Turner, A. Vishwanath, and S. Y. Savrasov, Topological semimetal and Fermi-arc surface states in the electronic structure of pyrochlore iridates, Phys. Rev. B **83**, 205101 (2011).
[6] S. M. Young, S. Zaheer, J. C. Y. Teo, C. L. Kane, E. J. Mele, and A. M. Rappe, Dirac Semimetal in

Three Dimensions, Phys. Rev. Lett. **108**, 140405 (2012).
[7] F. Wang and D.-H. Lee, Topological relation between bulk gap nodes and surface bound states: Application to iron-based superconductors, Phys. Rev. B **86**, 094512 (2012).
[8] Z. Wang, Y. Sun, X.-Q. Chen, C. Franchini, G. Xu, H. Weng, X. Dai, and Z. Fang, Dirac semimetal and topological phase transitions in A_3 Bi (A = Na, K, Rb), Phys. Rev. B **85**, 195320 (2012).
[9] A. Burkov, M. Hook, and L. Balents, Topological nodal semimetals, Phys. Rev. B **84**, 235126 (2011).
[10] For a review, see, e.g., M. Z. Hasan, C. L. Kane, Colloquium: Topological insulators, Rev. Mod. Phys. **82**, 3045 (2010).
[11] For a review, see, e.g., N. P. Armitage, E. J. Mele, A. Vishwanath, Weyl and Dirac semimetals in three dimensional solids, Rev. Mod. Phys. **90**, 15001 (2018).
[12] H. C. Po, A. Vishwanath, and H. Watanabe, Symmetry–based indicators of band topology in the 230 space groups, Nat. Commun. **8**, 50 (2017).
[13] J. Kruthoff, J. de Boer, J. van Wezel, C. L. Kane, and R.-J. Slager, Topological Classification of Crystalline Insulators through Band Structure Combinatorics, Phys. Rev. X **7**, 041069 (2017).
[14] L. Fu and C. L. Kane, Topological insulators with inversion symmetry, Phys. Rev. B **76**, 045302 (2007).
[15] H. Zhang, C.-X. Liu, X.-L. Qi, X. Dai, Z. Fang, and S.-C. Zhang, Topological insulators in Bi_2Se_3, Bi_2Te_3 and Sb_2Te_3 with a single Dirac cone on the surface, Nat. Phys. **5**, 438 (2009).
[16] Y. Xia, D. Qian, D. Hsieh, L. Wray, A. Pal, H. Lin, A. Bansil, D. Grauer, Y. S. Hor, R. J. Cava, and M. Z. Hasan, Observation of a large-gap topological-insulator class with a single Dirac cone on the surface, Nat. Phys. **5**, 398 (2009).
[17] H. Lin, L. A. Wray, Y. Xia, S. Xu, S. Jia, R. J. Cava, A. Bansil, and M. Z. Hasan, Half–Heusler ternary compounds as new multifunctional experimental platforms for topological quantum phenomena, Nat. Mater. **9**, 546 (2010).
[18] S. Chadov, X. Qi, J. Kübler, G. H. Fecher, C. Felser, and S. C. Zhang, Tunable multifunctional topological insulators in ternary Heusler compounds, Nat. Mater. **9**, 541 (2010).
[19] D. Xiao, Y. Yao, W. Feng, J. Wen, W. Zhu, X.-Q. Chen, G. M. Stocks, and Z. Zhang, Half-Heusler Compounds as a New Class of Three-Dimensional Topological Insulators, Phys. Rev. Lett. **105**, 096404 (2010).
[20] B. Yan, M. Jansen, and C. Felser, A large-energy-gap oxide topological insulator based on the superconductor $BaBiO_3$, Nat. Phys. **9**, 709 (2013).
[21] X. Zhang, H. Zhang, J. Wang, C. Felser, and S.-C. Zhang, Actinide topological insulator materials with strong interaction, Science **335**, 1464 (2012).
[22] M. Dzero, K. Sun, V. Galitski, and P. Coleman, Topological Kondo Insulators, Phys. Rev. Lett. **104**, 106408 (2010).
[23] R. Yu, H. Weng, Z. Fang, Xi Dai, and X. Hu, Topological Node-Line Semimetal and Dirac Semimetal State in Antiperovskite Cu_3PdN, Phys. Rev. Lett. **115**, 036807 (2015)
[24] Y. Kim, B. J. Wieder, C. L. Kane, and A. M. Rappe, Dirac Line Nodes in Inversion-Symmetric Crystals, Phys. Rev. Lett. **115**, 036806 (2015).
[25] Y. Du, F. Tang, D. Wang, L. Sheng, E.-J. Kan, C.-G. Duan, S. Y. Savrasov, and X. Wan, CaTe: A new topological node-line and Dirac semimetal, NPJ Quantum Mater. **2**, 3 (2017).
[26] Y. Du, X. Bo, D. Wang, E.-J. Kan, C.-G. Duan, S. Y. Savrasov, and X. Wan, Emergence of topological nodal lines and type II Weyl nodes in strong spin-orbit coupling system $InNbX_2$(X=S, Se), Phys. Rev. B **96**, 235152 (2017).
[27] J. Kanamori, Theory of the magnetic properties of ferrous and cobaltous oxides, Prog. Theor. Phys. **17**, 177 (1957).
[28] B. J. Kim, H. Ohsumi, T. Komesu, S. Sakai, T. Morita, H. Takagi, and T. Arima, Phase-sensitive observation of a spin-orbital mott state in Sr_2IrO_4, Science **323**, 1329 (2009).
[29] H. Weng, C. Fang, Z. Fang, B. A. Bernevig, and X. Dai, Weyl Semimetal Phase in Noncentrosymmetric Transition-Metal Monophosphides, Phys. Rev. X **5**, 011029 (2015).
[30] S.-M. Huang, S.-Y. Xu, I. Belopolski, C.-C. Lee, G. Chang, B. Wang, N. Alidoust, G. Bian, M. Neupane, C. Zhang, S. Jia, A. Bansil, H. Lin, and M. Z. Hasan, A Weyl Fermion semimetal with surface Fermi arcs in the transition metal monopnictide TaAs class, Nat. Commun. **6**, 7373 (2015).
[31] V. Aji, Adler-Bell-Jackiw anomaly in Weyl semimetals: Application to pyrochlore iridates, Phys. Rev. B **85**, 241101 (2012).
[32] D. T. Son and B. Z. Spivak, Chiral anomaly and classical negative magnetoresistance of Weyl metals, Phys. Rev. B **88**, 104412 (2013).
[33] K.-Y. Yang, Y.-M. Lu, and Y. Ran, Quantum Hall effects in a Weyl semimetal: Possible application in pyrochlore iridates, Phys. Rev. B **84**, 075129 (2011).
[34] S. A. Parameswaran, T. Grover, D. A. Abanin, D. A. Pesin, and A. Vishwanath, Probing the Chiral Anomaly with Nonlocal Transport in Three-Dimensional Topological Semimetals, Phys. Rev. X **4**, 031035 (2014).
[35] A. C. Potter, I. Kimchi, and A. Vishwanath, Quantum oscillations from surface Fermi arcs in Weyl and Dirac semimetals, Nat. Commun. **5**, 6161 (2014).
[36] J. Ruan, S.-K. Jian, H. Yao, H. Zhang, S.-C. Zhang, and D. Xing, Symmetry–protected ideal Weyl semimetal in HgTe-class materials, Nat. Commun. **7**, 11136 (2016).
[37] F. Ebert and H. Woitinek, Kristallstrukturen von Fluoriden, II. HgF, HgF_2, CuF und CuF_2, Z. Anorg. Allg. Chem. **210**, 269 (1933).
[38] R. W. G. Wyckoff, ZnS structure, sphalerite structure, *Crystal Structures*, 2nd ed. (Interscience, New York, 1963), Vol. 1, p. 85.
[39] M. Cardona, Optical properties of the silver and cuprous halides, Phys. Rev. **129**, 69 (1963).
[40] J. M. Crabtree, C. S. Lees, and K. Little, The copper fluorides: Part I-X-ray and electron microscope examination, J. Inorg. Nucl. Chem. **1**, 213 (1955).
[41] C. M. Wheeler, Jr. and H. M. Haendler, The thermal decomposition of copper (II) fluoride dihydrate, J. Am. Chem. Soc. **76**, 263 (1954).
[42] T. Fukui, Y. Hatsugai, and H. Suzuki, Chern numbers in discretized brillouin zone: Efficient method of computing (spin) Hall conductances, J. Phys. Soc. Jpn. **74**, 1674 (2005).
[43] A. A. Mostofi, J. R. Yates, G. Pizzi, Y. S. Lee, I. Souza, D. Vanderbilt, and N. Marzari, A tool for obtaining maximally-localised Wannier functions, Comput. Phys. Commun. **185**, 2309 (2014).
[44] D. Fischer, W. Carl, H. Glaum, and R. Hoppe, Zur Struktur der KAgO-Verwandtschaft Neubestimmung an

$AAgO = A_4[Ag_4O_4]$ (A = Na–Rb) mit einer Bemerkung zu CsCuO, Z. Anorg. Allg. Chem. **585**, 75 (1990).

[45] R. Umamaheswari, M. Yogeswari, and G. Kalpana, Electronic properties and structural phase transition in A4[M4O4] (A=Li, Na, K and Rb; M=Ag and Cu): A first principles study, Solid State Commun. **155**, 62 (2013).

[46] T. Gruhn, Comparative ab initio study of half-Heusler compounds for optoelectronic applications, Phys. Rev. B **82**, 125210 (2010).

[47] X. Huang, L. Zhao, Y. Long, P. Wang, D. Chen, Z. Yang, H. Liang, M. Xue, H. Weng, Z. Fang, X. Dai, and G. Chen, Observation of the Chiral-Anomaly–Induced Negative Magnetoresistance in 3D Weyl Semimetal TaAs, Phys. Rev. X **5**, 031023 (2015).

[48] G. Resta, S.-T. Pi, X. Wan, and S. Y. Savrasov, High surface conductivity of Fermi-arc electrons in Weyl semimetals, Phys. Rev. B **97**, 085142 (2018).

[49] P. Blaha, K. Schwarz, G. K. H. Madsen, D. Kvasnicka, and J. Luitz, *WIEN2K, An Augmented Plane Wave + Local Orbitals Program for Calculating Crystal Properties* (Technische Universitat Wien, Austria, 2001).

[50] F. Tran and P. Blaha, Accurate Band Gaps of Semiconductors and Insulators with a Semilocal Exchange-Correlation Potential, Phys. Rev. Lett. **102**, 226401 (2009).